iScience

CellPress
OPEN ACCESS

Article

In aqua dual selective photocatalytic conversion of methane to formic acid and methanol with oxygen and water as oxidants without overoxidation

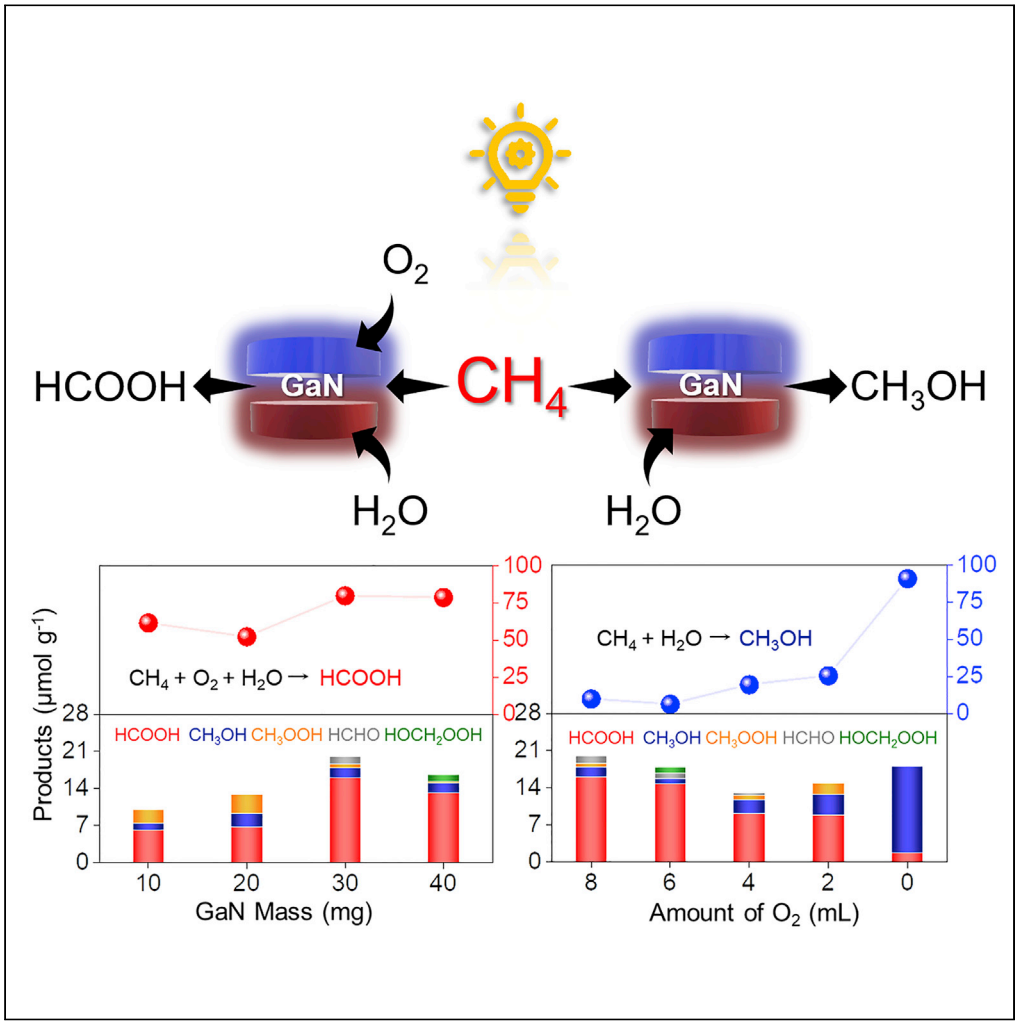

Jing-Tan Han, Hui Su, Lida Tan, Chao-Jun Li

cj.li@mcgill.ca

Highlights

Dual selective photoconversion of CH_4 into HCOOH and CH_3OH has been achieved by GaN

Selectivity toward oxygenates rather than CO_2 is maintained well with or without O_2

•OOH and •OH are generated in a controllable manner by GaN under UV light

Han et al., iScience 26, 105942
February 17, 2023
https://doi.org/10.1016/j.isci.2023.105942

iScience

CellPress
OPEN ACCESS

Article

In aqua dual selective photocatalytic conversion of methane to formic acid and methanol with oxygen and water as oxidants without overoxidation

Jing-Tan Han,[1,2] Hui Su,[1,2] Lida Tan,[1] and Chao-Jun Li[1,3,*]

SUMMARY

The direct and selective transformation of naturally abundant methane (CH_4) into high-value-added oxygenates, e.g., methanol, ethanol, and formic acid, is one of the "Holy Grails" in chemistry and chemical productions. However, complex mixtures of products, often due to over-oxidations, make such transformations highly challenging. Herein, gallium nitride (GaN), a methane-active semiconductor, catalyzes the photooxidation of methane and empowers the fine-controlling of chemoselectivity toward methanol and formic acids, simply by regulating the O_2 content in water. In contrast to previous methods, no overoxidation products (CO_2 and CO) were observed in this process. Mechanistic investigations and the corresponding quantitative experiments indicated that the controllable generation of moderately reactive oxygen radicals (●OOH and ●OH) in combination with the direct methane activation triggered by GaN is responsible for the highly selective reactivity and tunability through a photo-generated radical process.

INTRODUCTION

Methane (CH_4), due to its widespread existence in natural gas, biogas, shale gas, and ocean floors, has drawn immense attention in terms of its transportation, storage, and effective transformation because of its natural abundance as fuel and chemical feedstock as well as the strong greenhouse impact caused by its direct release into the atmosphere.[1,2] Developing novel and sustainable catalysis technologies for on-site methane liquefication into valuable liquid fuels[3–5] in the replacement of conventional off-site reforming processes has been a significant subject in the chemical and energy industries, especially in the syngas-dependent methanol and formic acid syntheses (Scheme 1A). The strategy of direct photocatalytic methane functionalization has been proposed as a promising alternative to circumvent issues of requiring harsh reaction conditions as well as over-oxidations often encountered in conventional thermal catalysis[6–8] and utilizing corrosive electrolyte in electro-catalysis.[9,10] In the state-of-art light-driven methane oxidation systems with oxygen and water as oxidant, methane-activation mainly relies on the assistance of photoexcited reactive oxygenated radicals (●OOH or ●OH) for cleaving C-H bond.[11–13] As expected, excessive oxidative species used for achieving high productivity unavoidably makes complicated and an uncontrollable mixture of oxygenated products. Therefore, realizing highly selective photoconversion into specific and useful oxygenated products remains a great challenge. Many kinds of semiconductors such as TiO_2, V/SiO_2, MoO_3, ZnO, WO_3, $BiVO_4$ and C_3N_4,[14–19] have been found their applications for partial photooxidations of methane with nitric oxide (NO), hydrogen peroxide (H_2O_2), and even molecular oxygen (O_2) as oxidants to generate commodity oxygenates such as methanol, ethanol, and formic acid.[20–22] To improve the photocatalytic efficiency of bare semiconductors, loading expensive noble metals (Au, Pd, Pt) and even binary metals (Au-Cu) on typical semiconductor-supports as photogenerated electron acceptors have enabled the conversion of methane into C_1 oxygenates with high selectivity and productivity.[21,23] Unfortunately, all these reported photocatalytic solutions are still confronted with great restriction on controlling specific liquid oxygenate product as well as suppressing overoxidation into CO_2. In this perspective, exploring a novel semiconductor-promoted photoinduced and selective methane oxidation into specific C_1 oxygenate, especially in absence of overoxidation, still needs to be unlocked. GaN-based catalysts with the feature of directly activating inert C-H bond in CH_4 have been successfully applied in thermal and photo dehydrogenation transformations of methane.[24,25] Such merit of GaN in breaking C-H bond makes it possible as a promising candidate to circumvent overoxidation toward selective CH_4 conversion. Herein, we present a dual selective conversion of methane into formic acid and methanol with molecular oxygen

[1]Department of Chemistry, and FRQNT Center for Green Chemistry and Catalysis, McGill University, 801 Sherbrooke Street West, Montreal, QC H3A 0B8, Canada

[2]These authors contributed equally

[3]Lead contact

*Correspondence: cj.li@mcgill.ca

https://doi.org/10.1016/j.isci.2023.105942

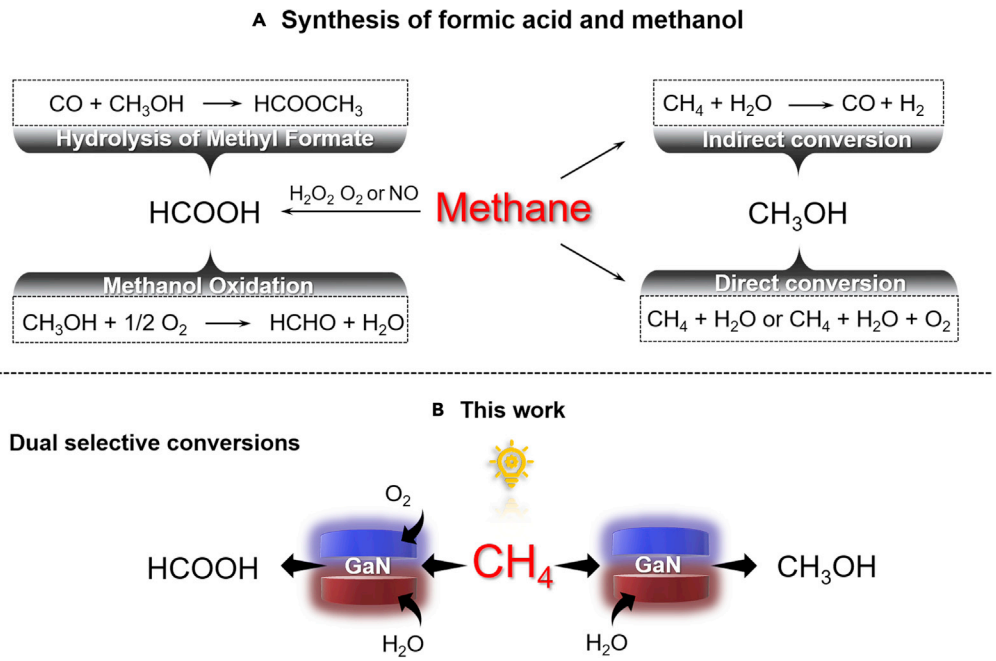

Scheme 1. Routes to synthesize HCOOH and CH_3OH from CH_4

(A) Traditional pathways for synthesizing HCOOH and CH_3OH.

(B) This work: the selective conversion of CH_4 to HCOOH and CH_3OH with oxygen and water as oxidants, respectively, under ambient conditions in water.

and water as oxidants, respectively, under ambient conditions in water accomplished by using the commercial GaN semiconductor for the first time. In this photocatalytic system, GaN, owing to its unique photophysical property and methane-activation ability can realize the specific production of methanol with ~90% selectivity or formic acid with ~80% selectivity by controlling the O_2 content in water. Namely, the primary product is methanol under O_2-free conditions and formic acid with O_2 in water. Mechanistic studies suggest that moderately reactive radicals of ●OOH and ●OH are generated in a controllable manner triggered by GaN-semiconductor under UV irradiation, which is primarily responsible for tuning the selectivity toward different C_1 products in sophisticated methane oxidation.

RESULTS AND DISCUSSION

Catalyst characterization

Apart from high chemostability, pale-yellowish commercial GaN powder affords representative semiconducting properties (Figure 1). First of all, a typical wurtzite crystalline structure of commercial GaN powder was well reflected by Powder X-ray Diffraction (XRD) patterns (Figure 1A). The rest of the peaks are attributed to the inevitable residual of Ga_2O_3 in the commercial GaN powder samples due to the high-temperature ammonization of Ga_2O_3 used for preparing gallium nitride in industry.[26,27] The high-resolution transmission electron microscopy (HRTEM) and their corresponding electron diffraction patterns further confirm that the polycrystalline GaN powder is mainly composed of the lattice fringe of c-planes (0001) and m-planes (1100) (supplemental information, Figure S1), which is consistent with our previous reported results.[25] As observed in photoluminescence (PL) spectrum (supplemental information, Figure S2), such commercial GaN semiconductor mainly has an obvious ultraviolent light emission from 300 nm to 410 nm with a corresponding band gap of 3.24 eV calculated from the DR UV-Vis result (Figure 1B). Combining with the X-ray photoelectron spectroscopy (XPS) valence band spectra (Figures 1C),[28] semiconducting band alignment of commercial GaN is identified. As shown in Figure 1D, the two-electron water oxidation potential and O_2 reduction potential to H_2O_2 locate between the top of the valence band (2.31 eV) and the bottom of the conduction band (−0.93 eV). Hence, GaN-semiconductor with sufficient redox capacity enables a compromise between activation energy barriers of both two-electron water oxidation and O_2 reduction to form H_2O_2 and related oxygen species *in situ*, which facilitates the subsequent indirect methane activation. Meanwhile, such a GaN-based protocol also provides a large room to further optimize reaction parameters for selective methane photooxidation toward specific products (supplemental information, Table S1).

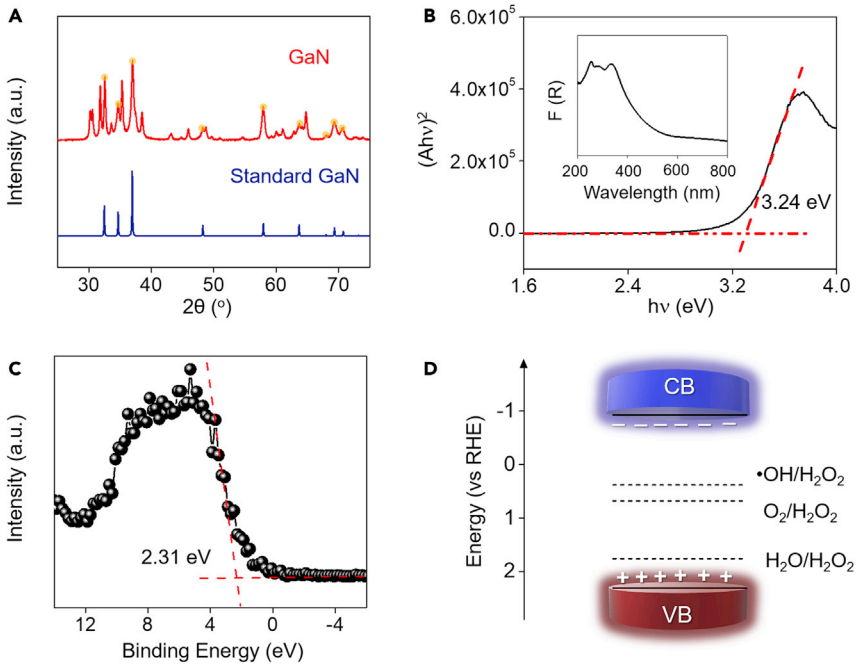

Figure 1. Band structure of commercial GaN semiconductor

(A) The XRD patterns of commercial GaN semiconductor and standard GaN.

(B) Tauc plots (Inset is diffuse reflectance (DR) UV-Vis spectra), (C) XPS valence band spectra, and (D) electronic band alignment of commercial GaN powder.

Catalyst performance

Based on our previous studies, the challenging polarization and cleavage of the C-H bond of CH_4 molecule can be promoted by GaN-based materials.[24,25] At the onset, we tested the photocatalytic performance of CH_4 oxidation with O_2 and water in a quartz tube reactor at room temperature (25 °C) under the irradiation of a 300 W Xenon lamp ($\lambda > 200$ nm). The conversion of methane to liquid oxygenates products did not take place in absence of light, methane, or using acetonitrile instead of water as solvent (supplemental information, Figure S3 and Table S2). Trace oxygenated mixtures but a large amount of CO_2 were observed under standard photocatalytic condition, in which methane gas was added but in absence of the catalyst (supplemental information, Figures S3 and S4 and Table S2). Strikingly, the introduction of GaN semiconductor results in the apparent generation of liquid oxygenates. The selectivity toward primarily C1 products reaches up to 99% in total including methanol (9.79%), methyl peroxide (3.80%), formaldehyde (6.66%), and formic acid (79.75%) (supplemental information, Figure S5, and Table S3, entry 2). The carbon atom in the oxygenates comes from methane as shown in the $^{13}CH_4$ isotopic experiment (supplemental information, Figure S6). More importantly, overoxidation products such as CO_2 and CO were not detected using GaN catalyst (supplemental information, Figures S5, S7, S8, and S23, Tables S3 and S4). In comparison, pure Ga_2O_3 exhibited more selectivity toward CO_2 under the same reaction conditions, which eliminates the positive effect of the residual Ga_2O_3 phase of commercial GaN powder on catalytical reactivity (supplemental information, Figures S7 and S8 and Table S4). All these results demonstrate that the GaN semiconductor catalyzed photoconversion of methane with O_2 into oxygenates can proceed in water in absence of apparent overoxidation.

In theory, enhancing the exposure of active GaN surface with methane can increase both the C_1 yield and the product selectivity by varying the catalyst loading (Figure 2A). Indeed, the total yield of C_1 liquid oxygenates was increased to 20.01 μmol g^{-1} cat from 12.16 μmol g^{-1} cat with increasing the mass transfer of reactants and GaN catalyst from 10 mg to 30 mg. Further increasing GaN catalyst mass to 40 mg did not improve either the yield or selectivity, because of the blocking from the extra sample to effective GaN surface (Figure 2A, supplemental information and Table S5). Likewise, the selectivity toward formic acid was also increased from 61.45% to 79.74% upon excitation for 8 h, owing to the balance between the generation rate of oxygen species and reactive oxygen species triggered $\cdot CH_3$ radicals. The selectivity of formic acid is maintained afterward (Figure 2B, supplemental information and Table S6). Using such reaction conditions,

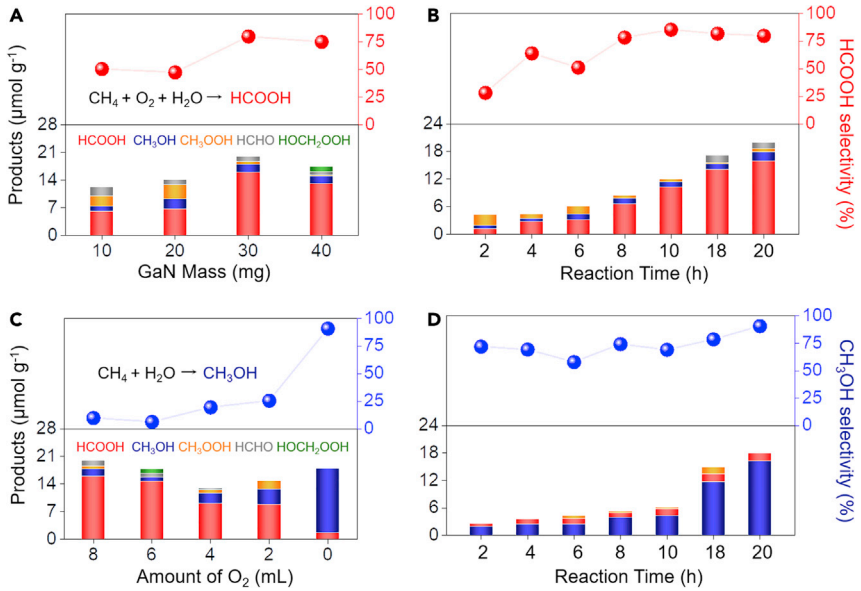

Figure 2. Selective methane photoconversion on GaN semiconductor

(A) The productivity and selectivity toward formic acid of GaN with O_2 over different catalyst masses and (B) corresponding time-dependent file with optimal GaN mass.

(C) The productivity and selectivity toward methanol of GaN with different O_2 amounts and (D) corresponding time-dependent file under O_2-free condition. Reaction conditions: 10-40 mg of photocatalyst, 1 mL of H_2O, 0-8 mL of O_2, 120 μmol of CH_4 under 1 atm, 25 °C, 300 W Xe lamp.

an optimal yield (16.01 μmol g cat^{-1}) and a high selectivity toward HCOOH (~80%) could be obtained after 20 h and maintained for 6 running cycles with a total 120 h (Figure 2B, supplemental information and Figure S9). The unchanged XRD patterns of fresh and used GaN samples demonstrated the structural stability of commercial GaN after 120 h reaction (supplemental information and Figure S10).

The switching of selectivity from formic acid to methanol can be achieved by gradually decreasing the amount of O_2 in the GaN-catalyzed photoconversion of methane in water (Figure 2C and supplemental information, Table S7). In absence of O_2, under otherwise the same conditions, continuous production of CH_3OH with 90.65% selectivity was achieved and maintained throughout the 20 h of reaction course (Figure 2D, supplemental information and Table S8). The corresponding yield of total C_1 oxygenates reaches up to 17.96 μmol g cat^{-1}, which is comparable to the one under O_2. The GaN semiconductor thus enables dual selective conversions of methane into formic acid and methanol, respectively, under aqueous media.

For comparison, the photocatalytic performances of other representative semiconductors such as ZnO, TiO_2, and g-C_3N_4 in the reported literature were investigated under identical conditions.[29–31] All three bare semiconductors showed much lower yields of oxygenates than GaN, among which the best performing g-C_3N_4 is merely 5.08 μmol g^{-1} cat, only approximately one-third of GaN (supplemental information, Figure S11 and Table S9). Furthermore, the overoxidation products of CO_2 from photoconversion of methane with water and O_2 over g-C_3N_4 were clearly observed after 20 h reaction while being barely noticeable in the GaN-catalyzed system (supplemental information, Figures S11 and S12 and Table S9). It is generally believed that because its oxidation potential is not enough to oxidize methane molecules, indirect activation of methane occurs on the surface of the g-C_3N_4 semiconductor upon excitation with the assistantance of water-generated oxidative radicals.[30] In sharp contrast, UV-sensitive GaN is able to grant easy access to methyl radical via the direct methane activation due to its strong oxidizing ability.[24] The results are also consistent with GaN's lower activation energy (24.49 kJ mol^{-1}) than that of g-C_3N_4 (53.16 kJ mol^{-1}) as calculated between 25 °C and 55 °C (supplemental information and Figure S13). These comparison experiments elucidate the advantage of GaN semiconductors in integrating direct and indirect activation of methane together, allowing photoinduced conversion of methane based on GaN with both high reactivity and product selectivity.

To examine the application potential for GaN-catalyzed methane conversion, we scaled up the reaction by utilizing a 120 mL air-tight quartz reactor. As expected, the total yield of C1 liquid oxygenates was

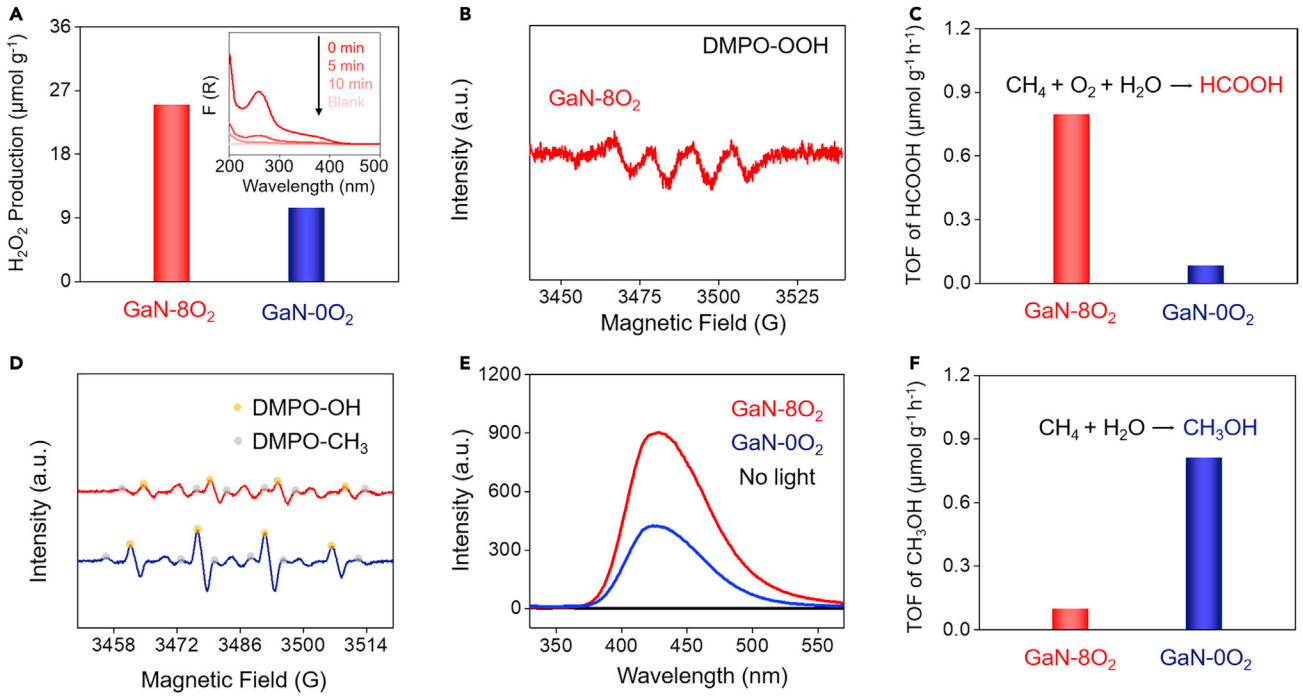

Figure 3. Mechanistic study

(A) Photocatalytic H_2O_2 production (Inset: absorbance of nitroblue tetrazolium chloride in O_2-promoted photodegradation reaction at different intervals) (B) EPR spectra of DMPO-OOH adduct and (C) corresponding TOF value of HCOOH over GaN for selective O_2-promoted (red) and O_2-free (blue) methane photooxidation.

(D) EPR spectra of DMPO-CH_3 and DMPO-OH under O_2-promoted and O_2-free photocatalytic condition.

(E) Fluorescence spectra of 2-hydroxyterephthalic acid for hydroxyl radical measurement with GaN under different reaction parameters.

(F) TOF value of CH_3OH over GaN for selective O_2-promoted and O_2-free methane photooxidation.

increased to 22.98 μmol g^{-1} cat from 4.28 μmol g^{-1} cat within 2 h under O_2-promoted reaction conditions (supplemental information and Table S10). More importantly, overoxidation products, including CO_2 and CO, are still not detected even after reacting 8 h with 0.54% of conversion and 71.52 μmol g^{-1} cat of C1 liquid oxygenates production (supplemental information, Figures S14 and S23). The low apparent quantum efficiency (AQE) of commercial GaN in O_2/O_2-free conditions at 370 nm could arise from the poor methane uptake of bulk GaN and limited methane solubility in water (supplemental information, Table S10).

Mechanistic study

Utilizing additional H_2O_2 as oxidant to trigger and facilitate methane cleavage for accessing methanol and methyl hydroperoxide through methane-methyl hydroperoxide-methanol pathway has emerged in low-temperature methane thermal conversion.[32] However, introducing different amounts of additional H_2O_2 into our photoconversion system, regardless of O_2-promoted or O_2-free condition, did not work as efficiently as previously reported examples.[22,31,32] The generation of primarily CH_3OOH and $HOCH_2OOH$ intermediates in these cases with external H_2O_2 led us to speculate that our selective methane photoconversion underwent a hydroperoxyl events (supplemental information, Figure S15 and Table S11).[32] Meanwhile, a notable drop in total yield of all liquid oxygenates and selectivity to either desired formic acid or methanol further establishes the irreplaceable role of *in situ* generated H_2O_2 on GaN surface, rather than external H_2O_2, in boosting the selective generation of methanol and formic acid (supplemental information, Figure S15 and Table S11). It is worth mentioning that under the O_2-promoted condition, two-electron O_2 reduction yields 24.99 μmol g cat^{-1} of H_2O_2, which is 2-fold of the one under the O_2-free condition (10.48 μmol g cat^{-1}) (Figure 3A). The effective generation of H_2O_2 is believed to be beneficial for the subsequent stage of generating active ●OOH radical (Figure 3A inset). Indeed, we identified a more pronounced ●OOH radical signal using 5, 5-dimethyl-1-pyrroline N-oxide (DMPO) as a spin trap with O_2 as co-oxidant compared to without O_2 (Figure 3B, supplemental information and Figure S16). As such, O_2 promoted *in situ* generation of ●OOH radical on the surface of GaN has a beneficial influence on boosting the

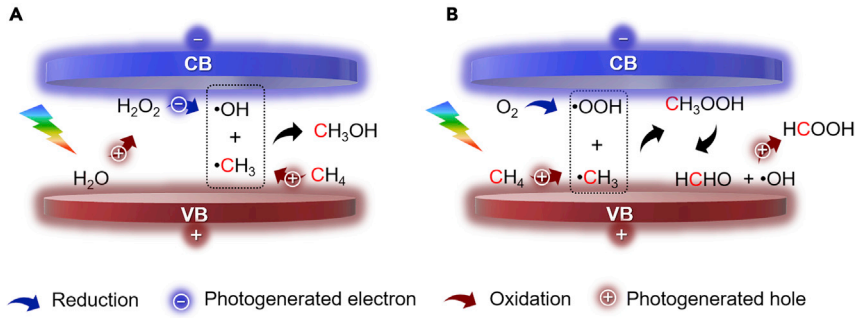

Figure 4. Proposed mechanism

Proposed reaction process toward the dual selective photoinduced conversion of CH_4 to (A) CH_3OH and (B) HCOOH over GaN semiconductor.

catalytic process toward the specific synthesis of formic acid with avoidance of overoxidation to CO_2 (Figure 3C).

In addition, further radical spin-trapping investigations found the concurrent existence of ●CH_3 and ●OH in the photocatalytic methane oxidation upon the irradiation of UV light, regardless of with or without O_2 (Figure 3D). Quantification analysis showed that more GaN-semiconductor photoinduced ●OH was generated with the increase of O_2 concentration due to the decomposition of more H_2O_2 (Figures 3E and 3A). However, the yield of primary oxygenates did not increase when increasing O_2, thus suggesting that ●CH_3 radical mainly results from the direct activation of methane triggered by photogenerated GaN hole (supplemental information, Figure S5 and Table S3). Considering the rapid coupling of ●CH_3 with moderate ●OH, selective production of methanol occurred in the case of O_2-free methane photooxidation with a TOF of 0.814 μmol g cat^{-1} h^{-1} for methanol, which is 8 times higher than that in the O_2-involved case (0.098 μmol g cat^{-1} h^{-1}) (Figure 3F). Therefore, it can be concluded that the concentration of reactive oxygen radical can be varied readily by varying the concentration of O_2, allowing to control the selective generation of oxygenated products.

Based on these experimental results above, a tentative mechanism for the dual selective photocatalytic CH_4 oxidation to formic acid and methanol under O_2 and O_2-free conditions catalyzed by GaN is shown in Figure 4. In the O_2-free case, initial H_2O photooxidation occurs at the photogenerated hole of GaN to form H_2O_2. Subsequently, ●OH derived from H_2O_2 decomposition,[33] can likely react with ●CH_3 generated on GaN to form methanol via direct radical coupling (Figures 4A and 4B, supplemental information and Table S12).[33] In O_2 involved case, excess ●OOH could convert ●CH_3 to HCHO via CH_3OOH arrangement step that would be further oxidized by ●OH into HCOOH (Figure 4B). (supplemental information, Table S13).[21,33–35]

Conclusions

In conclusion, a dual selective photoconversion of CH_4 to HCOOH or CH_3OH has been achieved for the first time, via GaN-catalysis with or without O_2 in water, in absence of overoxidation product. Photoexcited holes at the GaN surface exhibited the powerful oxidizing capacity to directly activate the methane C-H bond in the absence of O_2 for generating CH_3OH in an excellent selectivity of 90.65%. Furthermore, the enhanced generation of oxygen radical species such as ●OH and ●OOH in the presence of O_2 is established to drive the continuous oxidation of methanol into HCOOH with a selectivity of 79.75%. Beyond that, preliminary scaling-up experiments show a great commercial prospect over GaN photocatalyst by the way of loading GaN on a mesoporous solid support, such as zeolites or film, or running in a flow reactor. Accordingly, such a selectivity tunability toward specific oxygenated products based on GaN-semiconductor not only leads to the practical application of methane and natural gas utilizations[36,37] in the chemical and energy sectors but also opens a novel strategy for the development of semiconductor-prompted functionalization of C-H bonds.

Limitations of the study

The using of UV light is very critical for this reaction. If visible light is used as an alternative, there is basically no product output. In addition, bulk GaN has a limited surface area to realize more efficient adsorption of methane gas, resulting in a relatively lower apparent quantum efficiency.

STAR★METHODS

Detailed methods are provided in the online version of this paper and include the following:

- KEY RESOURCES TABLE
- RESOURCE AVAILABILITY
  - Lead contact
  - Materials availability
  - Data and code availability
- METHOD DETAILS
  - Materials
  - Small scale catalytic performance test
  - Large scale catalytic performance test
  - Catalytic stability test
  - Detection of hydroxyl radical (●OH)
  - Detection of superoxide radical (●OOH)
  - Quantification of hydrogen peroxide (H_2O_2)
  - GC-FID test for the quantification of CO_2
  - Quantifications and calculations of liquid products
  - Apparent quantum efficiency (AQE) measurement
  - Characterization

SUPPLEMENTAL INFORMATION

Supplemental information can be found online at https://doi.org/10.1016/j.isci.2023.105942.

ACKNOWLEDGMENTS

We thank the Natural Sciences and Engineering Research Council of Canada, Canada Research Chair program, Fonds de recherche du Québec – Nature et technologies, Canada Foundation for Innovations, and McGill University's MSSI fund for their support of our research. H.S. thanks Shanghai Jiao Tong University for SJTU Postdoctoral Award. We are thankful to Mahdi Salehi for the help with the GC-FID test, and Silvana Yin for the help with the AQE measurement.

AUTHOR CONTRIBUTIONS

Conceptualization, Li., C.-J.; methodology, Li., C.-J.; investigation, Han, J.-T., Su., H. and Tan, L., D.; writing – original draft, Han, J.-T. and Su., H.; writing –review & editing, Han, J.-T., Su., H., Tan, L., D., and Li., C.-J.; funding acquisition, Li., C.-J.; supervision, Li., C.-J.

DECLARATION OF INTERESTS

The authors declare no competing interests.

Received: September 22, 2022
Revised: December 7, 2022
Accepted: January 5, 2023
Published: February 17, 2023

REFERENCES

1. Ravi, M., Ranocchiari, M., and van Bokhoven, J.A. (2017). The direct catalytic oxidation of methane to methanol—a critical assessment. Angew. Chem. Int. Ed. Engl. *56*, 16464–16483. https://doi.org/10.1002/anie.201702550.

2. SherShah, M.S.A., Oh, C., Park, H., Hwang, Y.J., Ma, M., and Park, J.H. (2020). Catalytic oxidation of methane to oxygenated products: recent advancements and prospects for electrocatalytic and photocatalytic conversion at low temperatures. Adv. Sci. *7*, 2001946. https://doi.org/10.1002/advs.202001946.

3. Osadchii, D.Y., Olivos-Suarez, A.I., Szécsényi, Á., Li, G., Nasalevich, M.A., Dugulan, I.A., Crespo, P.S., Hensen, E.J.M., Veber, S.L., Fedin, M.V., et al. (2018). Isolated Fe sites in metal organic frameworks catalyze the direct conversion of methane to methanol. ACS Catal. *8*, 5542–5548. https://doi.org/10.1021/acscatal.8b00505.

4. Ab Rahim, M.H., Forde, M.M., Jenkins, R.L., Hammond, C., He, Q., Dimitratos, N., Lopez-Sanchez, J.A., Carley, A.F., Taylor, S.H., Willock, D.J., et al. (2013). Oxidation of methane to methanol with hydrogen peroxide using supported gold–palladium alloy nanoparticles. Angew. Chem. Int. Ed. Engl. *52*, 1280–1284. https://doi.org/10.1002/anie.201207717.

5. Kwon, Y., Kim, T.Y., Kwon, G., Yi, J., and Lee, H. (2017). Selective activation of methane on single-atom catalyst of rhodium dispersed on zirconia for direct conversion. J. Am. Chem. Soc. *139*, 17694–17699. https://doi.org/10.1021/jacs.7b11010.

6. Tomkins, P., Mansouri, A., Bozbag, S.E., Krumeich, F., Park, M.B., Alayon, E.M.C., Ranocchiari, M., and van Bokhoven, J.A.

(2016). Isothermal cyclic conversion of methane into methanol over copper-exchanged zeolite at low temperature. Angew. Chem. Int. Ed. Engl. *55*, 5467–5471. https://doi.org/10.1002/ange.201511065.

7. Meng, X., Cui, X., Rajan, N.P., Yu, L., Deng, D., and Bao, X. (2019). Direct methane conversion under mild condition by thermo-electro-or photocatalysis. Chem *5*, 2296–2325. https://doi.org/10.1016/j.chempr.2019.05.008.

8. Zhou, L., Martirez, J.M.P., Finzel, J., Zhang, C., Swearer, D.F., Tian, S., Robatjazi, H., Lou, M., Dong, L., Henderson, L., et al. (2020). Light-driven methane dry reforming with single atomic site antenna-reactor plasmonic photocatalysts. Nat. Energy *5*, 61–70. https://doi.org/10.1038/s41560-019-0517-9.

9. Nandenha, J., Fontes, E., Piasentin, R., Fonseca, F., and Neto, A. (2018). Direct oxidation of methane at low temperature using Pt/C, Pd/C, Pt/C-ATO and Pd/C-ATO electrocatalysts prepared by sodium borohydride reduction process. J. Fuel Chem. Technol. *46*, 1137–1145. https://doi.org/10.1016/S1872-5813(18)30046-X.

10. Yamanaka, I., Hasegawa, S., and Otsuka, K. (2002). Partial oxidation of light alkanes by reductive activated oxygen over the (Pd-black + $VO(acac)_2$/VGCF) cathode of H_2–O_2 cell system at 298 K. Appl. Catal. Gen. *226*, 305–315. https://doi.org/10.1016/S0926-860X(01)00916-4.

11. Cai, X., Fang, S., and Hu, Y.H. (2021). Unprecedentedly high efficiency for photocatalytic conversion of methane to methanol over Au–Pd/TiO_2–what is the role of each component in the system? J. Mater. Chem. *9*, 10796–10802. https://doi.org/10.1039/D1TA00420D.

12. Zhou, Y., Zhang, L., and Wang, W. (2019). Direct functionalization of methane into ethanol over copper modified polymeric carbon nitride via photocatalysis. Nat. Commun. *10*, 506–508. https://doi.org/10.1038/s41467-019-08454-0.

13. Wu, X., Zhang, Q., Li, W., Qiao, B., Ma, D., and Wang, S.L. (2021). Atomic-scale Pd on 2D titania sheets for selective oxidation of methane to methanol. ACS Catal. *11*, 14038–14046. https://doi.org/10.1021/acscatal.1c03985.

14. Kaliaguine, S., Shelimov, B., and Kazansky, V. (1978). Reactions of methane and ethane with hole centers O^-. J. Catal. *55*, 384–393. https://doi.org/10.1016/0021-9517(78)90225-7.

15. Thampi, K.R., Kiwi, J., and Grätzel, M. (1988). Room temperature photo-activation of methane on TiO_2 supported molybdena. Catal. letters *1*, 109–116. https://doi.org/10.1007/BF00765891.

16. Li, Z., Pan, X., and Yi, Z. (2019). Photocatalytic oxidation of methane over CuO-decorated ZnO nanocatalysts. J. Mater. Chem. *7*, 469–475. https://doi.org/10.1039/C8TA09592B.

17. Gondal, M.A., Hameed, A., and Suwaiyan, A. (2003). Photo-catalytic conversion of methane into methanol using visible laser. Appl. Catal. Gen. *243*, 165–174. https://doi.org/10.1016/S0926-860X(02)00562-8.

18. Zhu, W., Shen, M., Fan, G., Yang, A., Meyer, J.R., Ou, Y., Yin, B., Fortner, J., Foston, M., Li, Z., et al. (2018). Facet-dependent enhancement in the activity of bismuth vanadate microcrystals for the photocatalytic conversion of methane to methanol. ACS Appl. Nano Mater. *1*, 6683–6691. https://doi.org/10.1021/acsanm.8b01490.

19. Yang, J., Xiao, W., Chi, X., Lu, X., Hu, S., Wu, Z., Tang, W., Ren, Z., Wang, S., Yu, X., et al. (2020). Solar-driven efficient methane catalytic oxidation over epitaxial ZnO/$La_{0.8}Sr_{0.2}CoO_3$ heterojunctions. Appl. Catal. B Environ. *265*, 118469. https://doi.org/10.1016/j.apcatb.2019.118469.

20. Hu, Y., Higashimoto, S., Takahashi, S., Nagai, Y., and Anpo, M. (2005). Selective photooxidation of methane into methanol by nitric oxide over V-MCM-41 mesoporous molecular sieves. Catal. letters *100*, 35–37. https://doi.org/10.1007/s10562-004-3082-0.

21. Song, H., Meng, X., Wang, S., Zhou, W., Wang, X., Kako, T., and Ye, J. (2019). Direct and selective photocatalytic oxidation of CH_4 to oxygenates with O_2 on cocatalysts/ZnO at room temperature in water. J. Am. Chem. Soc. *141*, 20507–20515. https://doi.org/10.1021/jacs.9b11440.

22. Xie, J., Jin, R., Li, A., Bi, Y., Ruan, Q., Deng, Y., Zhang, Y., Yao, S., Sankar, G., Ma, D., and Tang, J. (2018). Highly selective oxidation of methane to methanol at ambient conditions by titanium dioxide-supported iron species. Nat. Catal. *1*, 889–896. https://doi.org/10.1038/s41929-018-0170-x.

23. Luo, L., Gong, Z., Xu, Y., Ma, J., Liu, H., Xing, J., and Tang, J. (2022). Binary Au–Cu reaction sites decorated ZnO for selective methane oxidation to C1 oxygenates with nearly 100% selectivity at room temperature. J. Am. Chem. Soc. *144*, 740–750. https://doi.org/10.1021/jacs.1c09141.

24. Li, L., Fan, S., Mu, X., Mi, Z., and Li, C.-J. (2014). Photoinduced conversion of methane into benzene over GaN nanowires. J. Am. Chem. Soc. *136*, 7793–7796. https://doi.org/10.1021/ja5004119.

25. Li, L., Mu, X., Liu, W., Kong, X., Fan, S., Mi, Z., and Li, C.-J. (2014). Thermal non-oxidative aromatization of light alkanes catalyzed by gallium nitride. Angew. Chem. *126*, 14330–14333. https://doi.org/10.1002/ange.201408754.

26. Kente, T., and Mhlanga, S.D. (2016). Gallium nitride nanostructures: synthesis, characterization and applications. J. Cryst. Growth *444*, 55–72. https://doi.org/10.1016/j.jcrysgro.2016.03.033.

27. Tyagi, A.K., and Banerjee, S. (2017). In Materials Under Extreme Conditions - Recent Trends and Future Prospects, V. Sudarsan, ed. (Elsevier), pp. 129–158.

28. Kraut, E.A., Grant, R.W., Waldrop, J.R., and Kowalczyk, S.P. (1980). Precise determination of the valence-band edge in x-ray photoemission spectra: application to measurement of semiconductor interface potentials. Phys. Rev. Lett. *44*, 1620–1623. https://doi.org/10.1103/PhysRevLett.44.1620.

29. Feng, N., Lin, H., Song, H., Yang, L., Tang, D., Deng, F., and Ye, J. (2021). Efficient and selective photocatalytic CH_4 conversion to CH_3OH with O_2 by controlling overoxidation on TiO_2. Nat. Commun. *12*, 4652–4710. https://doi.org/10.1038/s41467-021-24912-0.

30. Yang, Z., Zhang, Q., Ren, L., Chen, X., Wang, D., Liu, L., and Ye, J. (2021). Efficient photocatalytic conversion of CH_4 into ethanol with O_2 over nitrogen vacancy-rich carbon nitride at room temperature. Chem. Commun. *57*, 871–874. https://doi.org/10.1039/D0CC07397K.

31. Zhu, S., Li, X., Pan, Z., Jiao, X., Zheng, K., Li, L., Shao, W., Zu, X., Hu, J., Zhu, J., et al. (2021). Efficient photooxidation of methane to liquid oxygenates over ZnO nanosheets at atmospheric pressure and near room temperature. Nano Lett. *21*, 4122–4128. https://doi.org/10.1021/acs.nanolett.1c01204.

32. Agarwal, N., Freakley, S.J., McVicker, R.U., Althahban, S.M., Dimitratos, N., He, Q., Morgan, D.J., Jenkins, R.L., Willock, D.J., Taylor, S.H., et al. (2017). Aqueous Au-Pd colloids catalyze selective CH_4 oxidation to CH_3OH with O_2 under mild conditions. Science *358*, 223–227. https://doi.org/10.1126/science.aan6515.

33. Shi, S., Sun, Z., Bao, C., Gao, T., and Hu, Y.H. (2020). The special route toward conversion of methane to methanol on a fluffy metal-free carbon nitride photocatalyst in the presence of H_2O_2. Int. J. Energy Res. *44*, 2740–2753. https://doi.org/10.1002/er.5088.

34. Zhu, Y., Chen, S., Fang, S., Li, Z., Wang, C., and Hu, Y.H. (2021). Distinct pathways in visible-light driven thermo-photo catalytic methane conversion. J. Phys. Chem. Lett. *12*, 7459–7465. https://doi.org/10.1021/acs.jpclett.1c02053.

35. Sun, Z., Wang, C., and Hu, Y.H. (2021). Highly selective photocatalytic conversion of methane to liquid oxygenates over silicomolybdic-Acid/TiO_2 under mild conditions. J. Mater. Chem. *9*, 1713–1719. https://doi.org/10.1039/D0TA09226F.

36. Tan, L.-D., Su, H., Han, J., Liu, M., and Li, C.-J. (2022). Methane liquefaction: selective conversion of methane to cyclohexane via efficient surface-hydrogen-transfer catalyzed by GaN-supported platinum clusters. Sci. Report *12*, 18414. https://doi.org/10.1038/s41598-022-21915-9.

37. Dutta, K., Chaudhari, V., Li, C.-J., and Kopyscinski, J. (2020). Methane conversion to ethylene over GaN catalysts. Effect of catalyst nitridation. Appl. Catal. A, General *595*, 117430. https://doi.org/10.1016/j.apcata.2020.117430.

STAR★METHODS

KEY RESOURCES TABLE

REAGENT or RESOURCE	SOURCE	IDENTIFIER
Chemicals, peptides, and recombinant proteins		
Gallium Nitride (99.9% metals basis)	Alfa Aesar	Cat#40218; CAS: 25617-97-4
Methane (99.99% purity)	Air Liquide	REF#P1219L50R7A001; CAS: 74-82-8
$^{13}CH_4$ (99 atom% ^{13}C)	Sigma-Aldrich	Product Number: 490229; CAS: 6532-48-5
Oxygen (99.99% purity)	Praxair	CAS: 7782-44-7
Gallium (III) oxide (≥99.99% trace metals basis)	Sigma-Aldrich	Product Number: 215066; CAS: 12024-21-4
Titanium (IV) oxide, anatase (21 nm primary particle size (TEM), ≥99.5% trace metals basiss)	Sigma-Aldrich	Product Number: 718467; CAS: 13463-67-7
Zinc oxide (nanopowder, <100 nm particle size)	Sigma-Aldrich	Product Number: 544906; CAS: 1314-13-2
Graphitic Carbon Nitride	TCI	Product Number: G0539; CAS: 143334-20-7
Terephthalic acid (98% purity)	Sigma-Aldrich	Product Number: 185361; CAS: 100-21-0
Nitrotetrazolium blue chloride (≥90.0% ,HPLC)	Sigma-Aldrich	Product Number: N6876; CAS: 298-83-9
Potassium titanium oxalate	Sigma-Aldrich	Product Number: 14007; CAS: 14402-67-6
Dimethyl sulfoxide (anhydrous, ≥99.9%)	Sigma-Aldrich	Product Number: 276855; CAS: 67-68-5
Ammonium acetate (reagent grade, ≥98%)	Sigma-Aldrich	Product Number: A7262; CAS: 631-61-8
Acetic acid (ACS reagent, ≥99.7%)	Sigma-Aldrich	Product Number: 695092; CAS: 64-19-7
Pentane-2,4-dione (ReagentPlus®, ≥99%)	Sigma-Aldrich	Product Number: P7754; CAS: 123-64-6

RESOURCE AVAILABILITY

Lead contact

Further information and requests for resources should be directed to and will be fulfilled by the lead contact, Chao-Jun Li (cj.li@mcgill.ca).

Materials availability

All materials generated in this study are available from the lead contact without restriction.

Data and code availability

- The datasets and images generated during this study are available from the lead contact upon request.
- This paper does not report original code.
- Any additional information required to reanalyze the data reported in this paper is available from the lead contact upon request.

METHOD DETAILS

Materials

Commercial GaN catalyst (99.9% purity) were purchased from Alfa Aesar and used without further treatment. Methane (99.99% purity) was purchased from Air Liquide. $^{13}CH_4$ (99 atom% ^{13}C) were purchased from Sigma-Aldrich. Oxygen (99.99% purity) was purchased from Praxair. Other commercially available semiconductors (Ga_2O_3, TiO_2, ZnO) were purchased from Sigma-Aldrich and used without further purification. Graphitic carbon nitride (g-C_3N_4) was purchased from TCI and used without further purification. Terephthalic acid (98% purity), nitrotetrazolium blue chloride (≥90.0% HPLC), potassium titanium oxalate, dimethyl sulfoxide (anhydrous, ≥99.9%), ammonium acetate (reagent grade, ≥98%), acetic acid (ACS reagent, ≥99.7%) and pentane-2,4-dione (ReagentPlus®, ≥99%) were all purchased from Sigma-Aldrich.

Small scale catalytic performance test

Before performing the measurements, the catalyst was evacuated at 250°C for 2 h to remove water and other molecules adsorbed in the powders. In the CH_4 photocatalytic oxidation process, a suspension of deionized water (1 mL) with the corresponding amount of commercial GaN powder (10∼40 mg) was added to an air-tight quartz reactor (12 mL quartz tube). The reactor was then completely evacuated by oil pump after being frozen by liquid nitrogen, followed by the introduction of 3 mL CH_4 gas (0.3 bar) and corresponding amount of O_2 gas (0∼8 mL, 0∼0.7 bar) with syringes under room temperature. Afterwards, the reactor was partially submerged in a 25°C chiller and illuminated by a 300w full-arch Xe lamp (PE300 BUV) for 20 hours to complete the reaction. After the light irradiation, the gas products were qualitatively analyzed by gas chromatograph (Agilent 6890N Network Gas Chromatograph) equipped with thermal conductivity detector (TCD). The liquid products were quantified by nuclear magnetic resonance (Bruker Ascend 1 500 MHz Spectrometer) spectroscopy, in which dimethyl sulfoxide (DMSO, Sigma-Aldrich, 99.99%) was added as an internal standard.

Large scale catalytic performance test

Before performing the measurements, the catalyst was evacuated at 250°C for 2 h to remove water and other molecules adsorbed in the powders. In the CH_4 photocatalytic oxidation process, a suspension of deionized water (100 mL) with 100 mg commercial GaN powder was added to an air-tight quartz reactor (120 mL chamber reactor equipped with a quartz window). The reactor was then completely evacuated by oil pump after being frozen by liquid nitrogen, followed by the introduction of 0.3 bar CH_4 gas and corresponding amount of O_2 gas (0 bar or 0.7 bar) under room temperature. Afterwards, the reactor was partially submerged in a 25°C chiller and illuminated by a 300w full-arch Xe lamp (PE300 BUV). After the light irradiation, the gas products were qualitatively analyzed by gas chromatograph (Agilent 6890N Network Gas Chromatograph) equipped with TCD. For the case giving the best reaction performance, we analyzed the gas phase product by GC-FID equipped with methanizer. The liquid products were quantified by nuclear magnetic resonance (Bruker Ascend 1 500 MHz Spectrometer) spectroscopy, in which DMSO (Sigma-Aldrich, 99.99%) was added as an internal standard.

Catalytic stability test

For the stability test, the following procedure was carried out. Initially, fresh catalyst (30 mg of GaN powder) was used for the photocatalytic methane oxidation reactions. Upon completion of the first reaction cycle, the catalyst was separated from the reaction solution by a high-speed centrifuge and the catalyst is washed by distilled water 5 times in order to remove the surface-adsorbed reactants. Then 1 mL of deionized water was added into the sample, which was subsequently tested for another catalytic activity evaluation under the same reaction conditions, representing the second cycle of the catalyst. The rest can be done in the same manner, and the process was repeated 6 cycles.

Detection of hydroxyl radical (●OH)

For the ●OH detection, the formation of ●OH was monitored with terephthalic acid (98% purity, Sigma-Aldrich) as a probe, which could readily capture the radical to produce fluorescent 2-hydroxyterephthalic acid. The following procedure was carried out. 30 mg catalyst was dispersed in 1 mL of 0.5 mmol L^{-1} terephthalic acid dissolved into 2 mmol L^{-1} sodium hydroxide and kept stirring, then the reactor was frozen by liquid nitrogen, followed by the introduction of 0.3 bar CH_4 gas (3 mL) and corresponding amount of O_2 gas (0 or 0.7 bar, 0 or 8 mL) with syringes under room temperature. Fluorescence spectra of 2-hydroxyterephthalic acid after 1 h illumination was measured by spectrophotometer excited at 315 nm.

Detection of superoxide radical (●OOH)

For the●OOH detection, nitrotetrazolium blue chloride (NBT) was used as the probe molecule to detect ·OOH radicals. Typically, 30 mg GaN powder was mixed with 1 mL NBT solution (0.04 mM). Then the reactor was frozen by liquid nitrogen, followed by the introduction of 0.3 bar CH_4 gas (3 mL) and 0.7 bar O_2 gas (8 mL) with syringes under room temperature. The sample is then being stirred in dark for 30 min for the following irradiation. After irradiation for a specific length of time (0 min, 5 min, and 10 min), 1 mL of liquid product was mixed with 2.0 mL of water. The mixed solution was measured by Uv-vis adsorption spectroscopy.

Quantification of hydrogen peroxide (H_2O_2)

For the H_2O_2 test, the amount of H_2O_2 was determined by the potassium titanium oxalate spectrophotometric method. Briefly, 1 mL filtrate of liquid products from the suspension after 20 h irradiation was added into chromogenic reagent containing 1 mL of 0.12 mol L^{-1} potassium titanium oxalate solution and 1 mL of 0.055 mol L^{-1} sulfuric acid. The absorbance at 390 nm was detected on Uv-vis spectrophotometer.

GC-FID test for the quantification of CO_2

For the quantification of CO_2, 10 mL of gas products, obtained under the optimized reaction conditions (100 mg GaN, 10 mL H_2O, 0.3 bar CH_4, 0.7 bar O_2, 2 h), was analyzed by manual injection using gas chromatograph (GC, Clarus 590) equipped with methanizer and flame ionization detector.

Quantifications and calculations of liquid products

For the quantification of other liquid products (CH_3OH, HCOOH, CH_3COOH, $HOCH_2OOH$), ^1H NMR (Bruker Ascend 1 500 MHz Spectrometer) was used. Typically, 0.6 mL liquid product was mixed with 0.1 mL of D_2O, and 0.025 μL DMSO was added as an internal standard. The products were quantified by comparing the ^1H NMR signal of the products and the internal standard. The signal of protons from the solvent H_2O is much higher than that from the products. Therefore, all ^1H NMR spectra were recorded using a pre-saturation solvent suppression technique to suppress the dominant H_2O signal. For the quantification of HCHO, the amount of HCHO was determined by the colorimetric method. Briefly, 100 mL of reagent aqueous solution was first prepared by dissolving 15 g of ammonium acetate, 0.3 mL of acetic acid, and 0.2 mL of pentane-2,4-dione in water. Then, 0.5 mL of liquid product was mixed with 2.0 mL of water and 0.5 mL of reagent solution. The mixed solution was maintained at 35°C for 1 hour and measured by UV-vis adsorption spectroscopy until the adsorption intensity at 412 nm did not further increase.

$$\text{Yield} = \text{number of moles of (HCOOH + } CH_3OH + CH_3COOH + \text{HCHO + } HOCH_2OOH\text{) / Weight of catalyst}$$

$$\text{TOF value} = \text{number of moles of (HCOOH + } CH_3OH + CH_3COOH + \text{HCHO + } HOCH_2OOH\text{) / (Weight of catalyst) x (reaction time)}$$

Apparent quantum efficiency (AQE) measurement

For the AQE measurement, because the Xe lamp used in the standard procedure has a wide wavelength spectrum, we used a single wavelength 370 nm kessil lamp to conduct the experiment to measure the AQE of GaN under the scaling up reaction condition (100 mg GaN, 10 mL H_2O, 0.3 bar CH_4/0.7 bar O_2 and 0.3 bar CH_4/0 bar O_2, 48h.). The irradiation area was controlled to be $\pi*(2.5)^2$ cm^2, and the light intensity was measured to be 12.98 mW●cm^{-2} by a Model 843-R power meter (Newport Corporation) equipped with an 818-ST2-UV power detector. The AQE was calculated by the following equations4:

$$AQE = \frac{Ne}{Np} * 100\% = \frac{10^9 (N_A * \nu * K) * (h * c)}{(I * A * \lambda)}$$

N_e is the number of reaction electrons, Np is the number of incident photons, N_A is Avogadro's constant (6.02×10^{23} mol^{-1}), ν is reaction rate (mol s^{-1}), K is the charge transfer numbers, h is the Planck constant (6.62×10^{-34} J·s), c is the speed of light (3.0×10^8 m·s^{-1}), I is the intensity of the irradiation (W·m^{-2}), A is the irradiation area (m^2), and λ is the wavelength of the monochromatic light (nm).

Characterization

The bright field transmission electron microscopy (TEM) observations were carried out on FEI Tecnai G2 F20 S/TEM at accelerating voltage of 200 kV. The X-ray photoelectron spectroscopy (XPS) was conducted on an ESCALAB 250 X-ray photoelectron spectrometer with a monochromated X-ray source (Al Kα hv = 1486.6 eV), and the energy calibration of the spectrometer was performed using C 1s peak at 5284.8 eV. The powder X-ray diffraction (XRD) patterns were obtained on a Bruker DD8 Advanced diffractometer with Cu Kα radiation (λ=1.5418 Å). Gas chromatography-thermal conductivity detector (GC-TCD)

was conducted on an Agilent 6890N Network Gas Chromatograph using argon (Ar) as the carrier gas. Ultraviolet-visible (UV-vis) spectrometry was performed by Agilent Cary 5000 series UV-vis-NIR spectrometer. Fluorescence quenching was performed on VARIAN CARY Eclipse fluorescence spectrophotometer. The PL measurement was performed with either a 405-nm laser or a 325-nm He-Cd laser (Kimmon Koha) as excitation source. Electron paramagnetic resonance (EPR) spectroscopy measurement was performed on a Bruker Elexsys E580 X-band EPR Spectrometer.